IL NUOVO CIMENTO Vol. 31 C, N. 5-6 Settembre-Dicembre 2008
DOI 10.1393/ncc/i2009-10359-x

Large eddy simulation and laboratory experiments on the decay of grid wakes in strongly stratified flows

P. Fraunie([1])([*]), S. Berreba([1])([3]), Y. D. Chashechkin([2]), D. Velasco([2])([3]) and J. M. Redondo([3])([**])

([1]) *Université du Sud Toulon-Var and C.N.R.S - La Garde Cedex, France*
([2]) *Institut for Problems in Mechanics - R.A.S. 10, Pr. Vernadskovo 119426 Moscow, Russia*
([3]) *Departamento de Física Aplicada, Universidad Politècnica de Catalunya 08034 Barcelona, Spain*

(ricevuto il 30 Gennaio 2009; approvato il 20 Aprile 2009; pubblicato online il 27 Luglio 2009)

Summary. — A detailed analysis of the flow structure resulting from the combination of turbulence and internal waves is carried out and visualized by means of the Schlieren method on waves in a strongly stratified fluid at the Laboratory of the IPM in Moscow. The joint appearance of the more regular internal wave oscillations and the small-scale turbulence that is confined vertically to the Ozmidov length scale favours the use of a simple geometrical analysis to investigate their time-space span and evolution. This provides useful information on the collapse of internal wave breaking processes in the ocean and the atmosphere. The measurements were performed under a variety of linear stratifications and different grid forcing scales, combining the grid wake and velocity shear. A numerical simulation using LES on the passage of a single bar in a linearly stratified fluid medium has been compared with the experiments identifying the different influences of the environmental agents on the actual effective vertical diffusion of the wakes. The equation of state, which connects the density and salinity, is assumed to be linear, with the coefficient of the salt contraction being included into the definition of salinity or heat. The characteristic internal waves as well as the entire beam width are related to the diameter of the bar, the Richardson number and the peak-to-peak value of oscillations. The ultimate frequency of the infinitesimal periodic internal waves is limited by the maximum buoyancy frequency relating the decrease in the vertical scale with the anisotropy of the velocity turbulent r.m.s. velocity.

PACS 47.55.Hd – Stratified flows.
PACS 47.27.-i – Turbulent flows.
PACS 47.20.Ft – Instability of shear flows (*e.g.*, Kelvin-Helmholtz).

([*]) E-mail: Philippe.Fraunie@lseet.univ-tln.fr
([**]) E-mail: redondo@fa.upc.edu

1. – Introduction

The collapse and relaminarization of turbulence in a stratified flow is an important subject in the atmospheric and ocean sciences because most of the vertical fluxes are going to be unsteady and after a sharp peak of local mixing there will be long periods of decaying turbulence and these will eventually dominate the estimates of turbulent diffusion, especially those that generate irreversible molecular mixing. The coupled ocean-atmospheric boundary layer is often stratified both under the water surface by thermoclines or haloclines, and the lower part of the atmosphere, which is characterized by a strong interaction with the ocean surface may also be stratified. Large-scale atmospheric models rely on small-scale parameterisation of vertical mixing, and the ability to identify the local processes, which determine mixing, is very important in order to increase the accuracy of forecasting. Strongly stratified regions often reduce drastically the vertical transport due to the considerably amount of energy which is used in producing internal waves, so there is need to take into account the changing mixing efficiency of the process produced by waves. The dynamics of density interfaces is controlled by the mixing due to many different processes. Also, benthic boundary layer results from mixing near the bottom of the sea. These processes merge near coastal regions, where tides often produce fronts. Sometimes exchanges between two different masses of water are locally controlled by interfacial mixing. The same is true in estuaries and river basins where fresh river water is mixed with all seawater. The decay of stratified wakes is of great relevance for many processes ranging from pollution control to climate-related research like the CO_2 vertical exchange. In region of intense shear and density gradients, the interaction of internal waves with the small-scale structure of the turbulence is not well known, but the measurements of vertical mixing are fundamental for climate and weather forecasting.

Vertical overturns, produced by turbulence in density stratified fluids, can be quantified by the Thorpe displacements d_T, the maximum displacement length $(d_T)_{\max}$ and the Thorpe scale L_T [1, 2].

We may also define a length scale related to the vertical stratification Λ as

$$\rho(z) = \rho_0 \exp[-z/\Lambda], \qquad \Lambda = |\mathrm{d} \ln \rho / \mathrm{d}z|^{-1}. \tag{1}$$

So that the Brunt-Väisälä frequency is then

$$N = \sqrt{g/\Lambda}, \qquad N^2 = \frac{g}{\rho} \left| \frac{\mathrm{d}\rho}{\mathrm{d}z} \right|. \tag{2}$$

Sharp density interfaces eventually become linearly stratified as mixing occurs, we will compare the results of numerical and laboratory experiments investigating the role of internal waves in the dynamics of the collapse and relaminarization of the turbulence in stratified flows. The non-linear relationship between the fluxes and the gradients of density and velocity have been known to produce the Phillips-Posmentier effect [3-6] where local mixing in a stratified fluid sharpens density interfaces instead of smoothing them, [7, 8] presented laboratory experiments on grid turbulence aimed at measuring the mixing efficiency and although it was argued that internal waves were relevant, only now, thanks to Schlieren measurements, their role is clear. Next we describe the numerical model used and the LES small-scale turbulence parametrization. In sect. **3** the numerical results are presented. In sect. **4** the experiments are described and the main results are

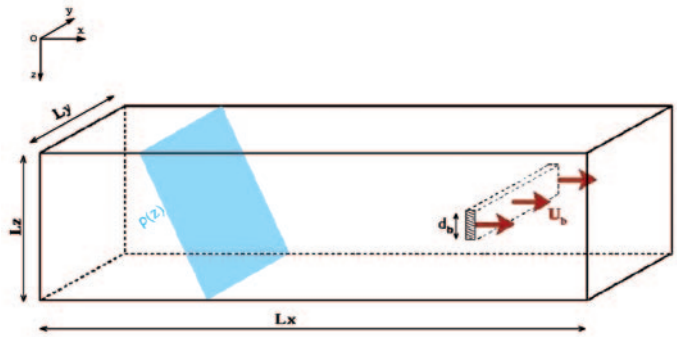

Fig. 1. – Numerical domain of size Lx, Ly, Lz, with a linear density profile.

highlighted, finally the stratified turbulence and the internal wave-vortex interaction is explained and the conclusions presented.

2. – Numerical method

The equations solved in the numerical model were the Navier-Stokes stratified-rotating ones with the Boussinesq approximation, which in terms of the buoyancy, b, may be expressed as

$$
\begin{aligned}
&\rho(b)\left(\frac{\partial \mathbf{u}}{\partial t} + (\mathbf{u}\nabla)\mathbf{u}\right) = -\nabla P + \nabla(\mu(b)\nabla\mathbf{u}) + \rho(b)(\mathbf{g} - 2\Omega \times \mathbf{u}),\\
&\frac{\partial b}{\partial t} + (\mathbf{u}\nabla)b = \nabla(\kappa_S(b)\nabla b),\\
&\operatorname{div}\mathbf{u} = 0, \quad \rho = \rho(b)
\end{aligned}
\tag{3}
$$

with the usual symbols, $\mu(b)$ and $\kappa_S(b)$ being the profiles of viscosity and solute diffusivity in terms of the total buoyancy b produced both by heat and or salt [9-12]. The rotation effects were ignored, considering that their role is not important for small-scale mixing. The numerical domain modelled the passage of a bar (horizontal or vertical) in a linearly stratified water tank, as seen in fig. 1 [13, 14]. The bar of side d_b is set at a speed U_b, and that produces a wake in the stably stratified fluid.

The scale $(L_T)_{\text{r.m.s.}} = L_T$ discussed in [1, 15] characterizes the vertical displacements of a stable density profile. By setting the buoyancy forces equal to the inertial forces, Ozmidov [7] derived a length scale L_O which would describe the largest possible overturning turbulent scale allowed by buoyancy as

$$
L_O = \sqrt{\frac{\varepsilon}{N^3}}, \tag{4}
$$

where ε is the kinetic energy dissipation rate and N the Brunt-Väisälä frequency. This relation is helpful to estimate mixing, at least that associated with patches of high turbulent activity [6, 16]. The Thorpe scale is nearly equal to the Ozmidov scale, L_O and they will set a limit on the vertical displacements on the lee of the bar wake.

The Richardson number, (Ri), measures the relative importance of buoyancy forces which usually act so as to stabilize the flow, and velocity fluctuations which tend to destabilize it. A bulk initial Richardson number (equivalent to the inverse square of the Froude number, F_x) can be defined as $Ri_b = F_x^{-2} = \frac{g'D}{U_b}$, g' being the reduced gravity $g' = \frac{\Delta\rho}{\rho}g$ for a sharp density interface, but we may define $\Delta\rho = (\mathrm{d}\rho/\mathrm{d}z)d_b$. The Richardson number can be defined in various ways and we will give appropriate definitions for each of the experimental situations investigated. The authors in [5, 6] defined a bulk Richardson number in terms of local parameters as

$$Ri_b = \frac{g\Delta\rho l}{\rho u'^2}\,, \tag{5}$$

where $\Delta\rho$ is the buoyancy jump across a density interface, u' is the turbulent velocity and l is an integral length scale of the turbulence defined as the area under the cross-correlation coefficient curve for the parallel velocity components. In general

$$l = \int_0^\infty R(\delta)\mathrm{d}\delta, \tag{6}$$

where δ is the distance between the density or velocity probes and $R(\delta)$ is the cross-correlation coefficient defined as

$$R(\delta) = \frac{\overline{u_i'(x)u_i'(x+\delta)}}{u'^2}\,. \tag{7}$$

In the model equations, which consider that the buoyancy is due to a combination of salt and heat is slightly more general, but cabelling has not been considered because a linear equation of state is used.

The values of the eddy diffusivity were explicitly separated in laminar and turbulent ones, both for momentum, salt and temperature, so the set of 5 equations for velocity components, v_i, average salinity and average temperature are

$$\begin{aligned}
&\frac{\partial\overline{v}_i}{\partial t} = -\overline{v}_j\frac{\partial\overline{v}_\mathrm{i}}{\partial x_j} - \frac{1}{\rho_0}\frac{\partial\overline{P}_d}{\partial x_i} - (1-\delta_{i3})\frac{g}{\rho_0}\int_0^z \frac{\partial\overline{\rho}}{\partial x_i}(x,y,z')\mathrm{d}z' + 2\frac{\partial}{\partial x_j}\left[(\nu+\nu_t)\,\overline{T}_{ij}\right],\\
&\frac{\partial\overline{S}}{\partial t} = -\overline{v}_j\frac{\partial\overline{S}}{\partial x_j} + \frac{\partial}{\partial x_j}\left[(\kappa+\kappa_t)\,\frac{\partial\overline{S}}{\partial x_j}\right],\\
&\frac{\partial\overline{T}}{\partial t} = -\overline{v}_j\frac{\partial\overline{T}}{\partial x_j} + \frac{\partial}{\partial x_j}\left[(\kappa_T+\kappa_{Tt})\,\frac{\partial\overline{T}}{\partial x_j}\right],
\end{aligned} \tag{8}$$

with T_{ij} the turbulent stress tensor and the lower index "t" indicating the turbulent viscosity or diffusivities.

The numerical method used was a time marching of three-steps Runge-Kutta scheme, with third-order accuracy in the spatial discretization and second-order centered finite differences.

The LES used a Smagorinski turbulent viscosity as

$$v_t(x,y,z,t) = (C_s\delta)^2\left|(SijSji)^{1/2}\right|, \tag{9}$$

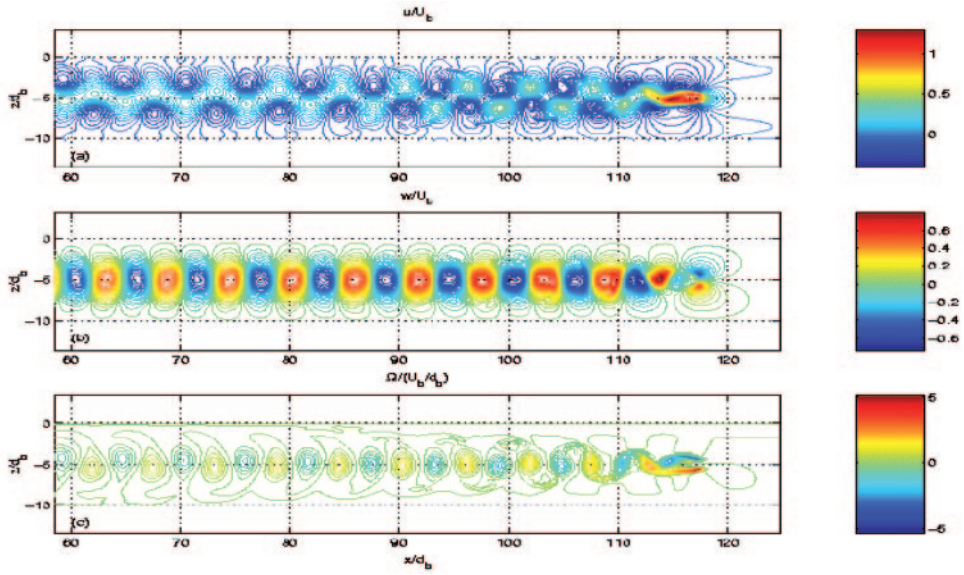

Fig. 2. – Values of the horizontal and vertical velocities (above) as well as the sideways vorticity (below).

with the length scale related to the numerical mesh $\delta = \sqrt[3]{\delta x \delta y \delta z}$. The relationship between the turbulent diffusivity and the turbulent viscosity is modelled empirically through a variable turbulent Schmidt number, Sc_t, as $\kappa_t = \frac{\nu_t}{Sc_t}$. For low Richardson numbers a linear relationship may be used but because Sc_t, that may be related to a mixing efficiency, varies in a strong non-linear fashion as demonstrated by Linden [5] and Redondo *et al.* [8,16].

3. – Numerical results

There is an increase of vertical displacements as the bar starts to move and a combination of small-scale turbulence and internal waves is produced behind the grid bar. Figures 2 and 3 show such process. The results are presented as centreline vertical planes normalized in x, the direction of the bar with its size as x/d_b. The top figures in fig. 2 represent the horizontal and vertical components of the velocity normalized with the velocity of the bar: u/U_b, and w/U_b. The lower figure in fig. 2 represents the value of the spanwise vorticity normalized as: $\Omega d_b/U_b$.

Observing fig. 2 for an intermediate-to-low Richardson number of $Ri = 0.05$ the trapped wave structure may be identified, the growth of the wake is monotonic between 60 to 120 x/d_b. The size of the vortices is also seen to grow with distance (or time) from the grid bar passage.

In fig. 3 a comparison of the vorticity contours for three different Richarson numbers numerical experiments is presented. The shape of the wakes may be outlined from the spanwise vorticity in the wakes of the three different numerical experiments with initial numbers $Ri_0 = 0.015$ (top), $Ri_0 = 0.1$ (centre), and $Ri_0 = 0.25$ (bottom). The Reynolds number is $Re = 880$, for all the experiments. The bar size is $d_b = 2\,\mathrm{cm}$, and its velocity $U_b = 4.4\,\mathrm{cm/s}$. Clearly the higher the Richardson number, the stronger the collapse. The

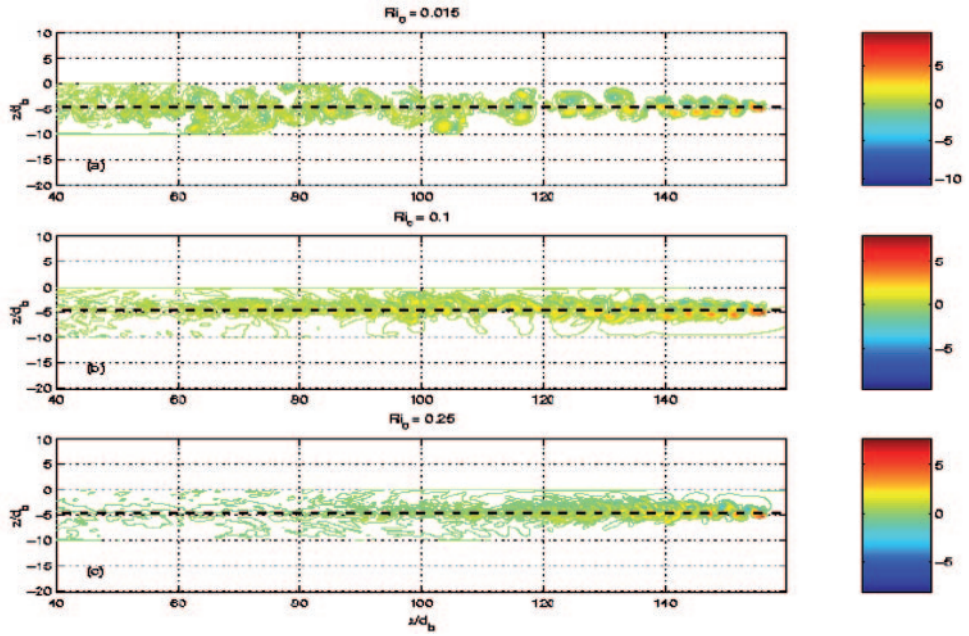

Fig. 3. – Comparison of the spanwise vorticity in the wakes of three different numerical experiments with initial numbers $Ri_0 = 0.015$ (top), $Ri_0 = 0.1$ (centre), $Ri_0 = 0.25$ (bottom). The Reynolds number is $Re = 880$. The bar size is $d_b = 2\,\mathrm{cm}$, and its velocity $U_b = 4.4\,\mathrm{cm/s}$.

waves observed are not so regular as in fig. 2 and after a region of growth of the wake, a decrease occurs. At the same time there is a decrease in the amplitude of oscillations of the vertical and horizontal velocities as well of their derivatives. Figure 4 also represents the velocity and the velocity derivatives in time. The damped oscillations observed are typical of the passage of an internal wave disturbance. This behavior can also be observed in fig. 5, which is similar to the two top plots in fig. 3 and represents the horizontal and vertical velocities, but with the fundamental difference that this time the bar is vertical instead of horizontal. Alternate signs on the velocities in zig-zag shape are typical and their vertical extent if forced by the turbulence collapse at scales larger than the Ozmidov (or Thorpe) length scale.

The observed collapse and relaminarization of the stratified flow is related, but not identical for vertical and horizontal bars as a comparison of figs. 3 and 5 shows, and this is important when comparing with experimental results, where mostly square grids are used [16-18].

Video digitizing and image analysis is a very promising technique nowadays for extended quantitative measurements at different scales both in space and time. Advanced fluid dynamics analysis from ImaCalc and DigiFlow programs as well as Eulerian density conductivity data will be used to further investigate the role of stratification on the stratified flow decay and relaminarization. The differences in stratification both in the LES simulations and in the laboratory experiments are parametrized with the local Richardson number as defined by [5, 16]. The clearest effect is that vertical (and horizontal) effective diffusivities vary over more than a decade. These measurements are reflected in the entrainment as discussed below in the discussion.

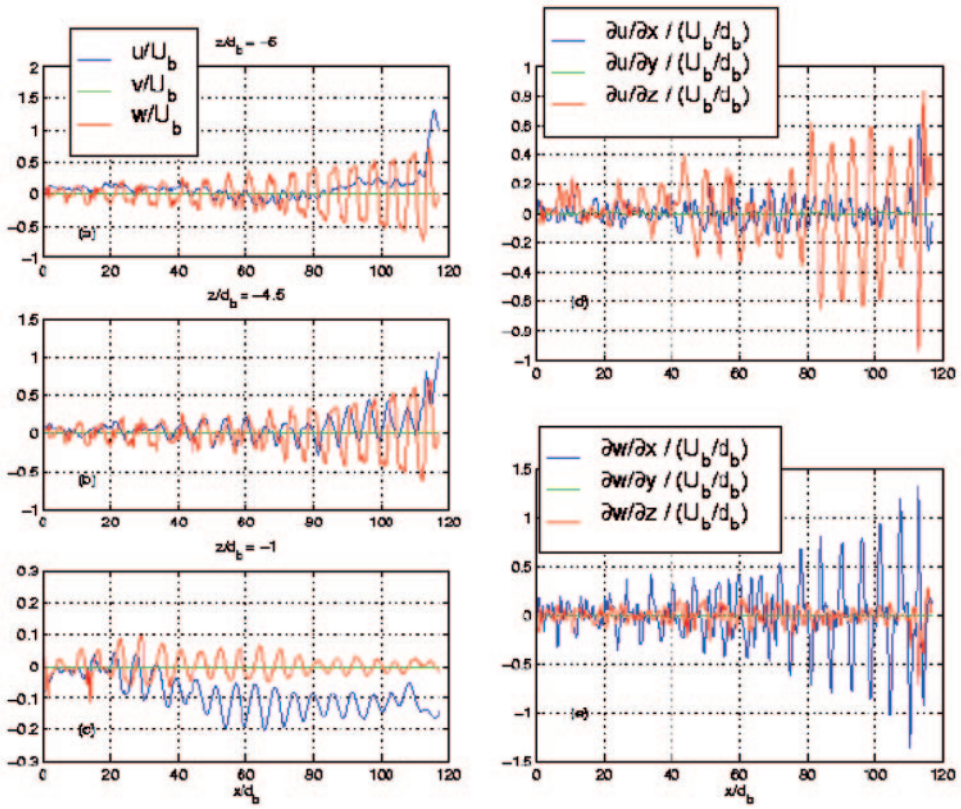

Fig. 4. – Variations behind the single horizontal grid bar of the velocity and its spatial local derivatives, which indicate the structure of the wake, $U_b = 4.4\,\mathrm{cm/s}$ is the mean bar velocity.

Figure 6 represents the normalized thickness of the wake for a single horizontal bar being displaced at uniform speed in the linearly stratified fluid. Five different Richardson numbers are compared, showing an initial vertical growth of the wake followed by a collapse of the normalized wake size behind the bar passage. The times Nt, where the start of the collapse takes place, are between 1.5 and 5 Nt. The increase of the wake size follows a common power law with power 1.3, but the behavior of the collapse in time depends on the Richardson number. The collapse takes place sooner the higher the Richardson number, but when the Brunt-Väisälä frequency is used to non-dimensionalize the data the behavior is not so clear. On the other hand, fig. 6 shows that when the Ozmidov scale has been reached collapse starts independently of the local Richardson number. Quite interesting in the numerical simulations is the clear role of internal wave propagation that should reduce the mixing efficiency in general, but probably in a non-linear fashion as discussed by [5, 16, 19, 20].

More results concerning the LES may be found in [20-22]. Considering the temporal evolution of the near wake width for Richardson numbers less than 1/4 the wake grows following a $t^{1/3}$ law as for a homogeneous flow. Then the collapse occurs when the wake width is maximum of about the Ozmidov scale. After that the wake width decreases up to a constant value with strong internal wave activity.

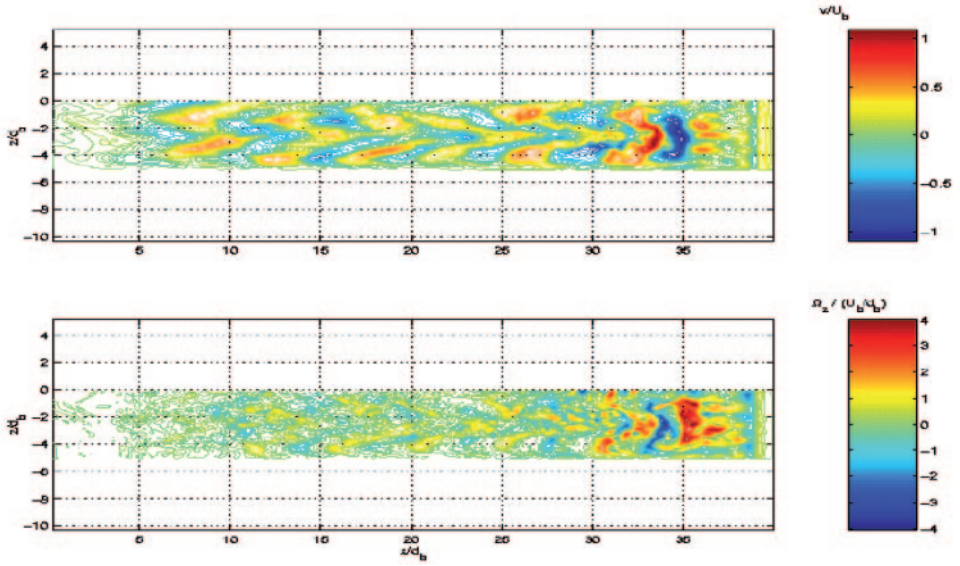

Fig. 5. – Structure of the collapse of the wake produced by a single vertical bar, here the local Ozmidov scale prevents vertical displacements. Top: vertical velocity, bottom: local vertical vorticity normalized by U_b/d_b.

The parameter $N_B V_t$ is used to normalize the maximum wake width H_m. The behavior depends on Ri_0 [20, 21] in the following fashion: for values of the local initial Richardson number $Ri_0 < 1/9\, H_m/N_B V_t$ varies in the range 1.5-2.5. For $1/9 < Ri_0 < 1/4\, H_m/N_B V_t$ varies between 3 and 5 and for more strongly stratified flows, $Ri_0 > 1/4$, the wake width is constant. This is another indication that the internal wave radiation of energy is much more important than previously thought [1, 5].

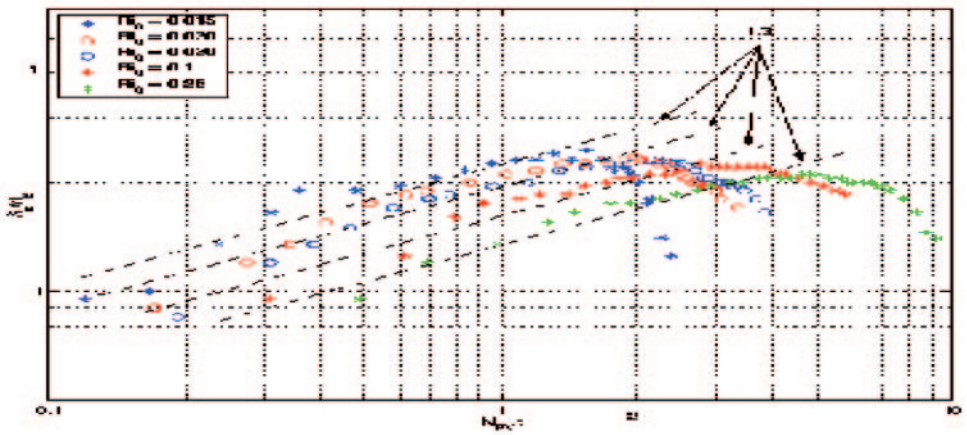

Fig. 6. – Collapse of the wake size behind the bar after the passage of a horizontal bar *vs.* time normalized with the Brunt-Väisälä frequency, Nt. The actual start of the collapse takes place between 1.5 and 5 Nt.

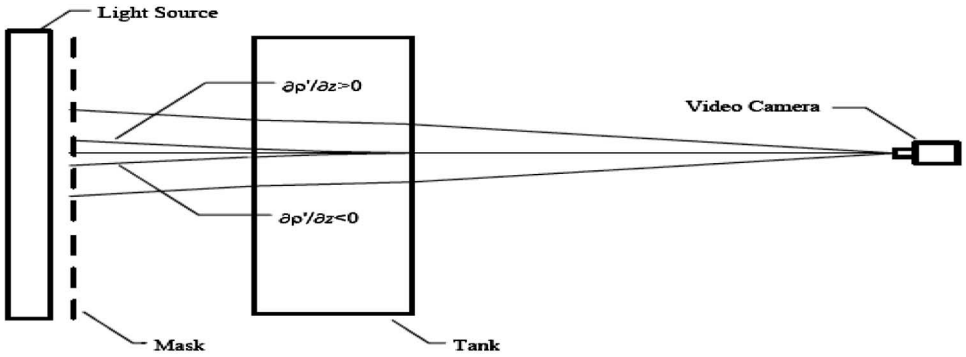

Fig. 7. – Detail of the synthetic Shlieren set-up at DAMTP, Cambridge.

4. – Experimental method and results

A series of experiments on the mixing structure of a sheared and grid stirred density interface were performed by [16], and more recent experiments including new measurements with a three-dimensional ADV sonic velocity and micro-density conductivity measurements have been done at DAMTP in Cambridge. The scale-to-scale transfer and the structure functions are examined and from these the intermittency parameters. The estimates of turbulent diffusivity could also be measured using neutrally buoyant Pliolite particles without significant external forces. Some two point correlations and time lag calculations are used to investigate the time and spatial integral length scales obtained from both Lagrangian and Eulerian correlations and functions, and we compare these results with both theoretical and experimental ones. The results presented here will complement the LES numerical simulations presented above to further investigate the collapse of a wake in a stratified (linear) flow and the wave field induced. This has been able to be measured using the IPM laboratory facilities in Moscow.

In sect. **3** we have defined the Thorpe scale, from measured displacements of the density profiles [15] as

$$(L_T)_{\text{r.m.s.}} = \left\langle d_T^2(z) \right\rangle^{1/2}. \tag{10}$$

The measurements on the maximum width of mixing grids of various sizes (mostly square) have been done by means of laser-induced fluorescente LIF and also by Schlieren both at DAMTP at Cambridge University and in Moscow. In fig. 7 the used synthetic Schlieren system is explained.

A detailed analysis of the flow structure resulting from the combination of turbulence and internal waves is visualized by means of real optical Schlieren of wakes in a strongly stratified fluid at the Laboratory of the IPM in Moscow. The joint appearance of the more regular internal wave oscillations and the small-scale turbulence that is confined vertically to the Ozmidov length scale favors also the use of multiscale-fractal analysis, but here we will limit to show the evidence for internal wave dissipation.

The experimental stratified shear flume used in Cambridge is shown in fig. 8 and the facility used in Moscow is shown in fig. 9. The visualizations shown, together with the LES numerical experiments, are only partial approximations to some of the type of real

Fig. 8. – Race track type of shear-stratified tank designed by [16] used for the LIF visualizations and the conductivity measurements on grid collapse. Above: general view, below: details of the disk pump.

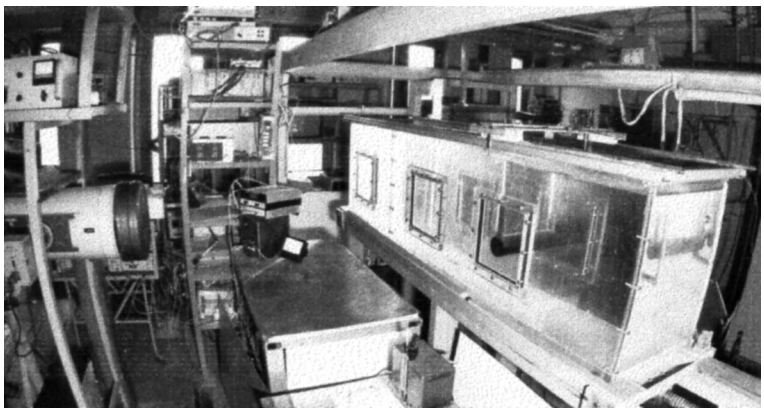

Fig. 9. – Large stratified tank used at IPM in Moscow, described in [17, 18, 31]. Experimental apparatus used for the internal wave measurements in this paper.

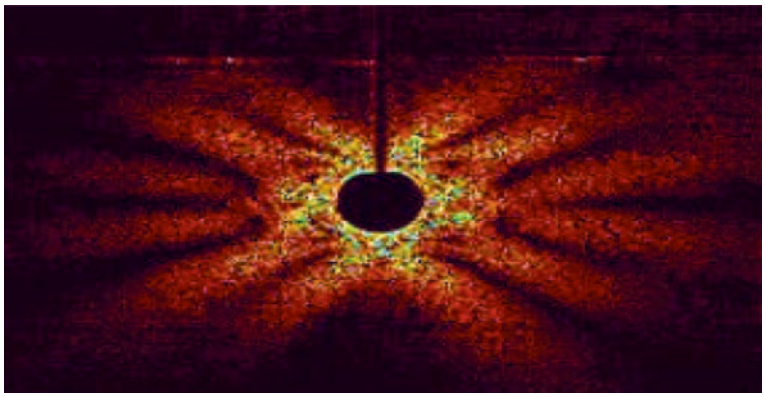

Fig. 10. – Image of the internal wave radiation with synthetic Schlieren.

complex features detected in environmental flows [23-25], such as intermittency related to non-homogeneity and stratification. Their time-space span and location provides useful information in the interpretation of internal wave breaking processes in the ocean and the atmosphere.

In both Cambridge and Moscow, the image registration was carried out by photo and video cameras having a spatial resolution better than 0.1 mm. The images obtained were digitized to a personal computer and then transformed and processed by means of ImaCalc and DigiFlow that allowed to obtain successive-frame photographic images and to measure the geometric characteristics of the flow components. Also they allow to make complex time and spatial quantitative measurements.

After the tank had been filled with the stratified solution and had been held for 24 h in order to decay all stratification non-homogeneities arising in filling in with the two-tank method, the buoyancy frequency was determined. Then, the grid or bar set up and the contact electric-conductivity sensors introduced measuring profiles and point Eulerian measures in time. To measure internal waves, the Schlieren system was used, and oscillation frequencies in the range $N = 0.43$–1.1 allow a variety of Richardson numbers also modified by the speed of the horizontal bar or grid. After the registration and measurement cycle were completed, the tank was let to rest and the new experiment started 1 to 2 h after ceasing of the motion and the decay of all disturbances in the tank, which had been registered by optical and conductivity probes.

The process of mixing across a density interface in zero mean flow may be used as a benchmark of sub-grid parametrization of turbulence models. It is important to predict whether a certain density interface subject to strong turbulence is going to be eroded and the gradients will weaken or, on the contrary, the gradients will increase at certain positions and a layered system will appear. Oscillating grid experiments have been used often [26,27] in the context of the evaluation of entrainment through heat and salt sharp interfaces. The entrainment laws for heat, sugar and salt have been also compared and their respective small-scale vertical and horizontal scales investigated both with grid wakes or/and with shear following [28-31].

The internal wave patterns shown by Schlieren are very revealing when they try to interpret the mixing efficiency measurements of [16] as well as the LES results shown in sect. **3**. Figures 10 and 11 show examples of the synthetic and optical Schlieren with the

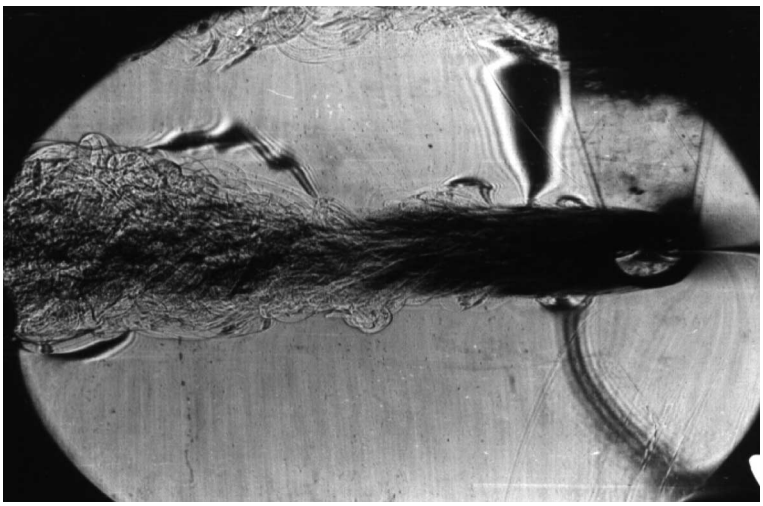

Fig. 11. – Image of the internal wave collapse in a very strongly stratified flow (experiment performed at Moscow Institute of Problems in Mechanics).

much better resolution of the second one. The type of dispersion relation as deduced by [30] shows clearly the non-linear interaction between the waves:

$$\left[\left(\omega + i\kappa_s k^2\right)\left(\omega + i\nu k^2\right) k^2 - N^2\left(k_x^2 + k_y^2\right)\right]\left(\omega + i\nu k^2\right) = 0. \tag{11}$$

Figure 12 shows a sequence of color enhanced images of the wake after a bar, the radiation of internal waves is apparent. It may be appreciated that the length scale of the internal waves slowly decreases outside the mixing and collapsing region. Inside this region that confirming the LES numerical experiments is smaller than the Ozdidov scale, we can also appreciate that the striations (fossil type of turbulence) are finer and finer in time. As the Batchelor scale is still much smaller, no further irreversible molecular mixing seems to take place. Density profiles of this area show a fractal structure [32-34].

From a video sequence of images such as those shown in fig. 12, a horizontal line in time and a vertical line in time near the centre of the image are shown in figs. 13 and 14. Here the full extent of the wake growth following a 1/3 power law as in the LES simulations is followed by the collapse of the core of the linearly stratified wake. What is observed, but not modelled correctly in the LES simulation, is the non-linear complexity of the internal wave field. For example, wave pairing and non-linear interactions are seen in regions with a really high Richardson and a very low Reynolds numbers. This will be discussed later when other results are presented in a (Ri, Re) parameter space. In order to do this, it is useful to revert to other visualization technique, LIF, that may be used to trace the different types of instability occurring at a sharp density interface. Even being quite sharp, the initial interfaces set up in the stratified-shear re-circulating tank, the internal mixing eventually produces a linear region inside the interfacial region that has a thickness λ. The thickness follows a similar power law with the Richardson number in grid strirred experiments and in shear-stratified mixing experiments, which was defined by [26]

$$\frac{\lambda}{\ell} = cRi^{-a}. \tag{12}$$

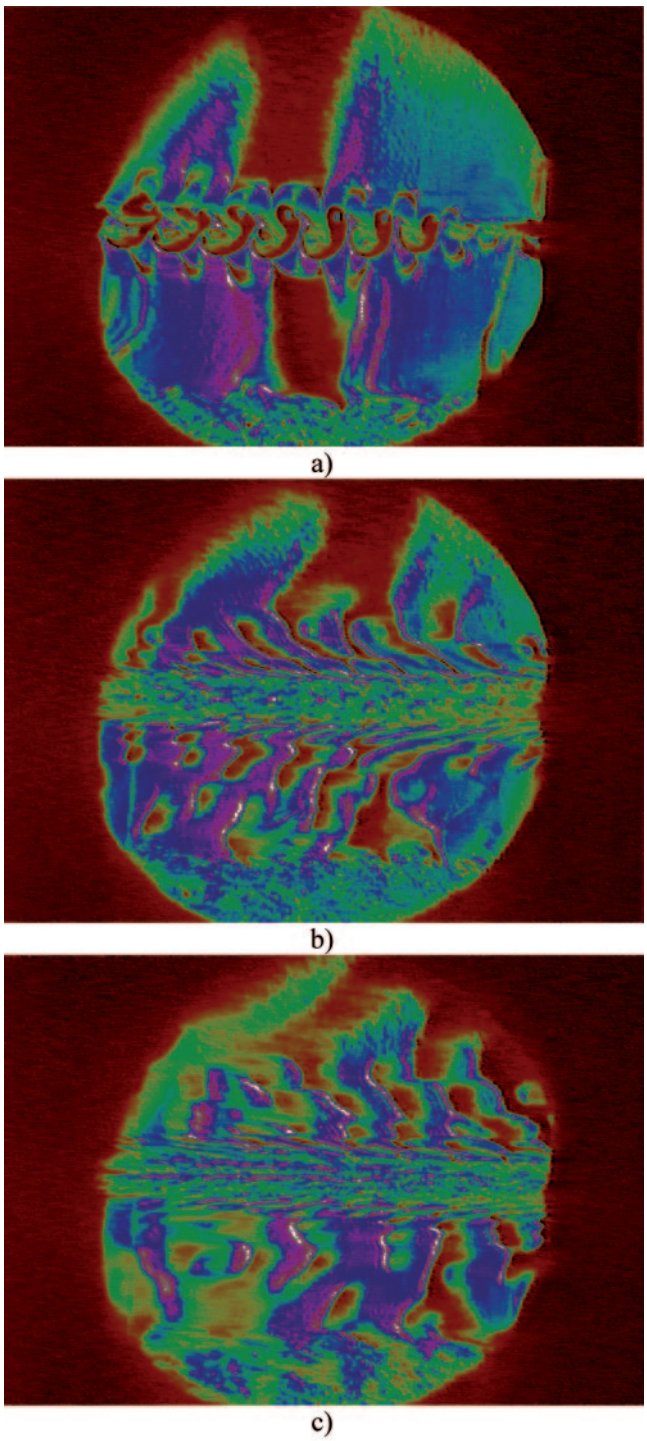

Fig. 12. – Sequence of Schlieren images of the flow visualization of the decay of the turbulence at a linear density interface. The collapsed inner region is clearly distinguished among the outer internal wave field.

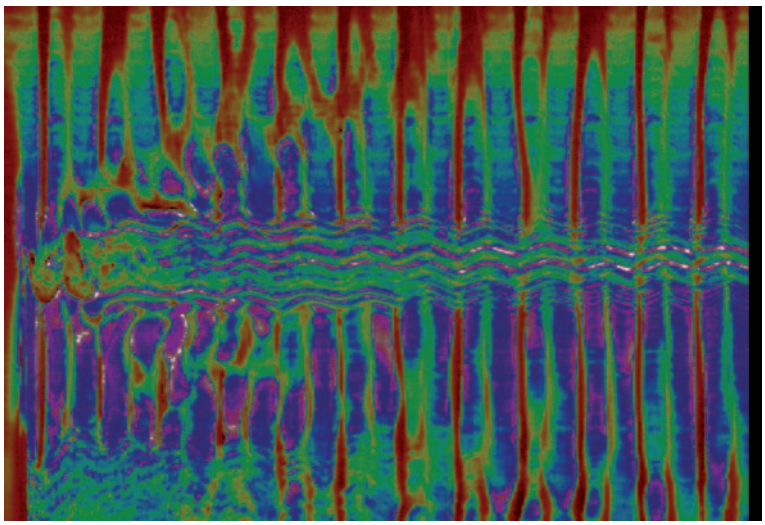

Fig. 13. – Time series of a vertical line during 100 s at 50 Hz of the passage of a horizontal bar in a linear stratification. Red and blue show the crests and troughs of the internal waves (density derivative).

The LIF visualizations show for a wide range of experiments, which are the dominant types of instabilities that correspond to different values of the local Reynolds number and the local Richardson number, for example in fig. 15 three types of patterns are shown when fluoresceine is used to mark one side (the dense salty one) of the interface: fig. 15a) shows an internal wave travelling trapped along the sharp interface, fig. 15b) shows the beginning of a Kelvin-Helmholtz billow and fig. 15c) shows some Holmboe-type streaks being lifted.

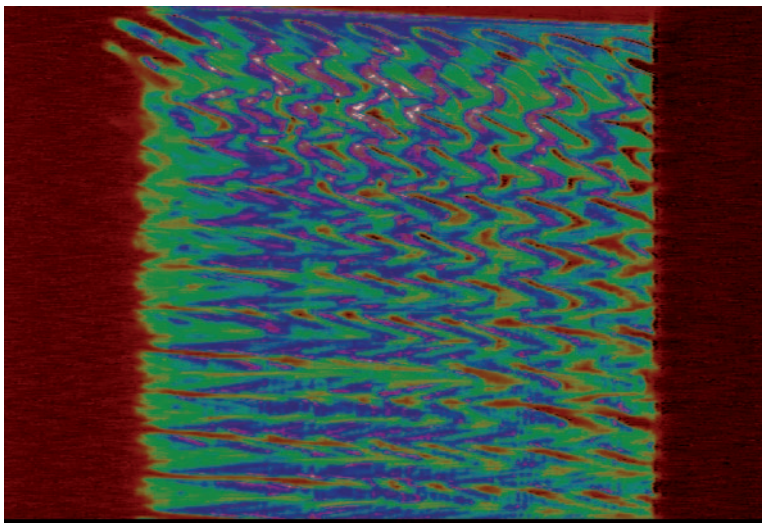

Fig. 14. – Time sequence (at 50 Hz) of Schlieren flow visualization of a horizontal line of the decay of the turbulence at a linear density stratification.

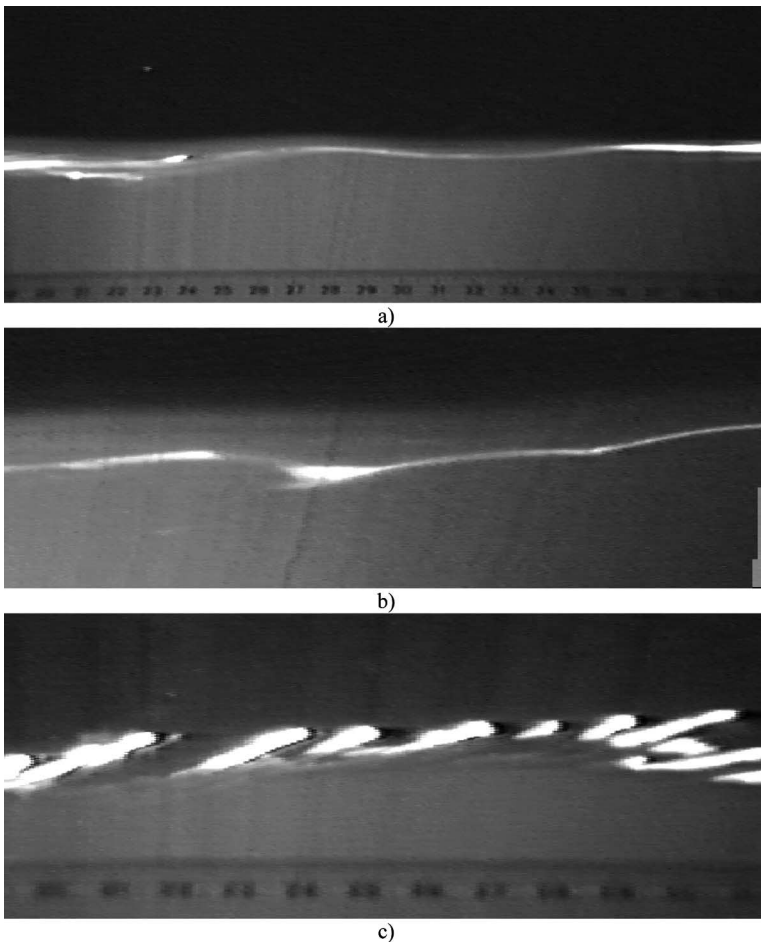

Fig. 15. – LIF images of different instabilities at a sharp density interface. a) High Ri, low Re, internal wave, b) medium Ri, high Re, Kelvin-Helmholtz Billow, c) medium Ri, medium Re, Holmboe instability.

In fig. 16 the time sequence of the appearance of several Holmboe instabilities during a shear stratified evolution of a density interface is shown. These instabilities are characterized by their cusps. As the Reynolds number is larger and the Richardson number smaller, the local Ozmidov (and Thorpe) scale is larger and the cusps are able to fully overturn, leading to a full Kelvin-Helmholtz billow [1]. As the Richardson number decreases, the cusps are elongated further and eventually Kelvin-Helmholtz instability develops. Figure 17 shows the roll up sequence of such a case.

5. – Discussion

As shown in sect. **4** for all experiments, both in bar and grid wakes, and in shear-generated mixing of a density interface, the maximum extent of the interfaces gets smaller as the local Richardson number increases, following eq. (12) we can add the new experiments with Schlieren to those by LIF of a sharp density [16, 26, 27].

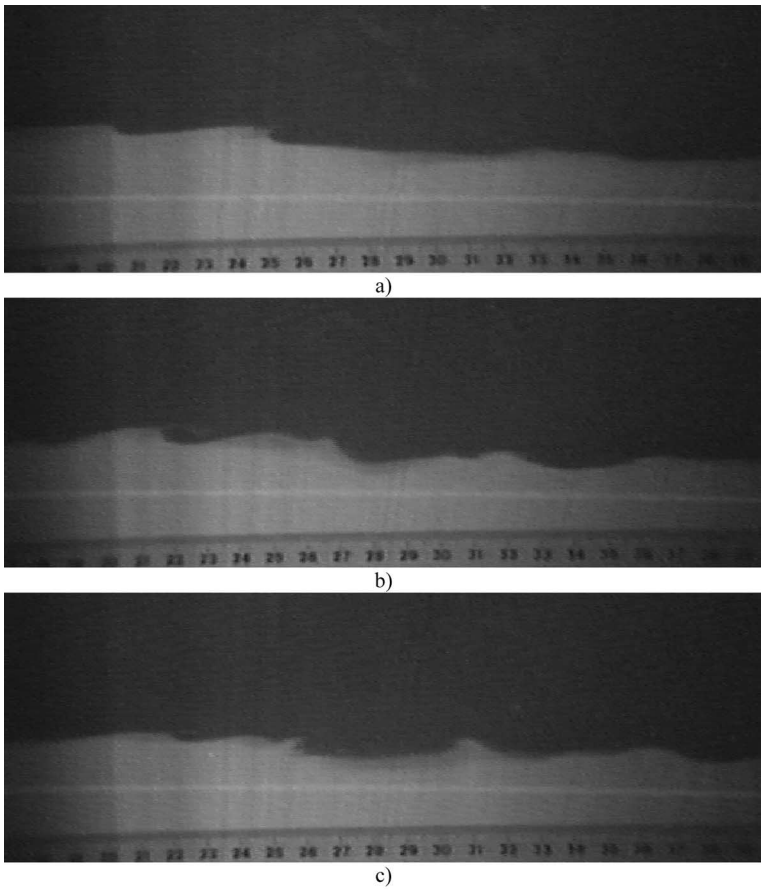

Fig. 16. – Laser-induced fluorescence flow visualization of the effect of the shear-generated turbulence at a sharp density interface. The intermediate Ri, Re of the experiment has the conditions for Holmboe instability development.

In the oscillating grid experiments [16], it was set to oscillate with fixed frequency and stroke at the beginning of the experiment and the velocity of advance of the interface V_e was measured by looking at a shadowgraph or by video recording of LIF. The turbulent parameters Ri and Re are derived from previous measurements of the integral turbulence scale from eq. (6) as a function of the distance between the grid center and the interface z as: $\ell = 0.1z$ and the turbulent velocity u' decays inversely proportional to the distance z. There are several mechanisms that produce mixing across the density interface, and there is also a dependence of the Prandtl number on the entrainment law.

In fig. 18 the dependence between the thickness of a density interface and the local Richardson number is presented confirming the validity of eq. (12) with possible different values for c and a. For most of the data the best fit is $a = 2/3$.

Figure 19 shows another type of visualization, pearlescence tracers, of the evolution of a sharp density interface after the passage of a grid. Here as with the Schlieren visualizations the internal waves are more apparent. When using shadowgraph, the internal waves are not apparent due to the fact that the second derivative of the density

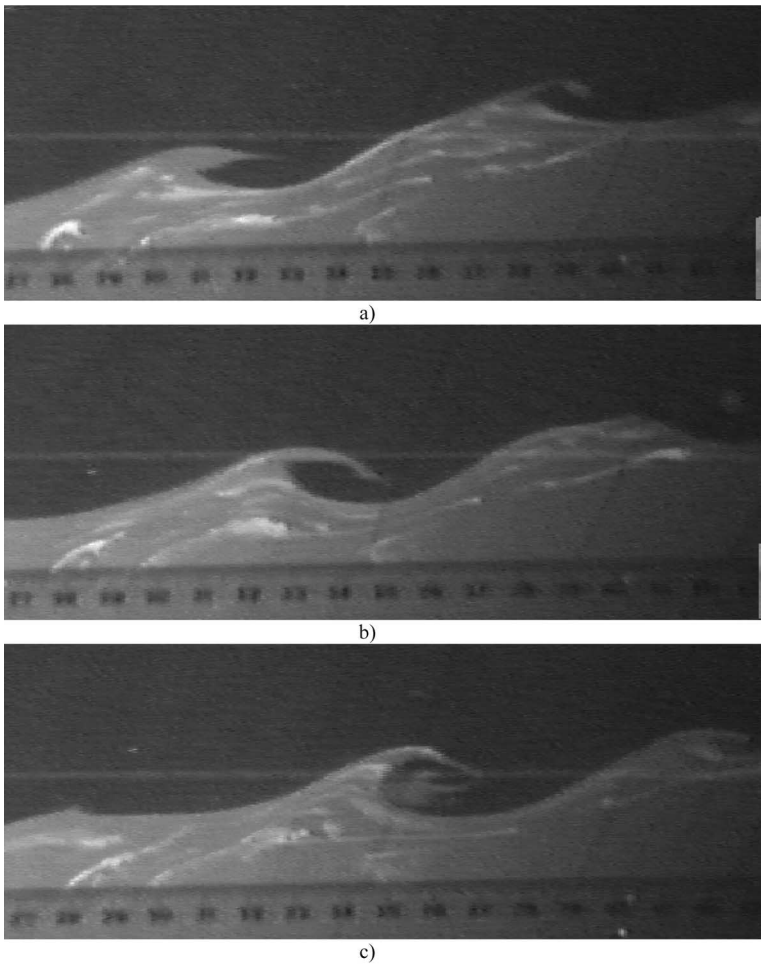

Fig. 17. – LIF flow visualization of the formation of a Kelvin-Helmholtz billow.

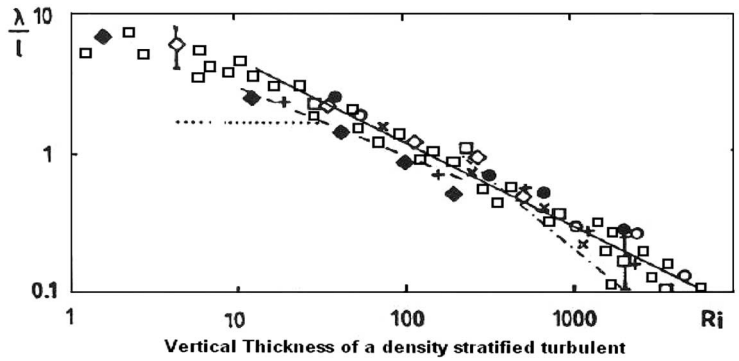

Fig. 18. – Non-dimensional thickness of a density interface subject to oscillating grid turbulence on one side of the interface adapted from [16]. Different symbols correspond to different grid frequencies.

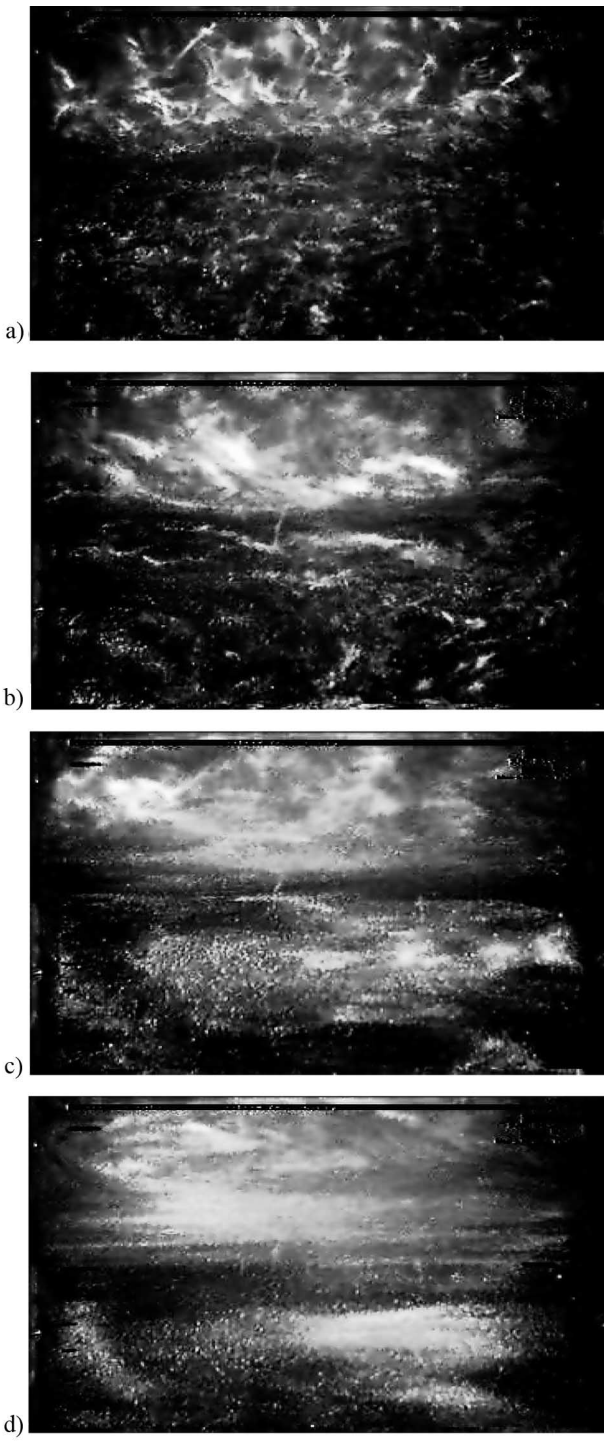

Fig. 19. – Pearlescence flow visualization of the decay of the turbulence at a sharp density interface. The collapse times measured in terms of the Brunt-Väisälä frequency are a) N, b) $2N$, c) $5N$, d) $10N$; $Ri = 30$.

field is what is actually visualized. So some earlier misguided ideas about the decay of a density interface or stratified flow were due to limited measurements.

For oscillating grid experiments Turner [35] proposed that the entrainment velocity Ue defined as $Ue = \mathrm{d}D/\mathrm{d}t$, where D is the depth of the turbulent layer, is given by a simple law of the form

$$E \propto Ri^{-n} \tag{13}$$

and found that the value of n in the entrainment equation was 3/2 when the stratification was due to salt, and 5/3 when was due to sugar, but the density-stratification resulted from a temperature gradient, the value of n was found to be close to 1. Turner also suggested that viscosity differences cannot be used to explain the different values of n, and proposed that the differences in Ve that occur when using salt and heat as the stratifying agents can only be explained by consideration of the molecular diffusion of mass and heat as defined by the appropriate diffusivity κ, and proposed that the entrainment velocity would be a function of both the Richardson number and the Peclet number $Pe = \frac{u'l}{\kappa}$. Turner initially suggested that $E \propto Ri^{-1}$, which he found for temperature stratification was the basic entrainment law, but he also found $E \propto Ri^{-3/2}$, for salt stratification, showing the influence of the molecular diffusivity on turbulent transport.

The entrainment measured in the grid stirred experiments [16] as a function of the Richardson number confirms Turner's [35] results showing power law dependence with $n = 3/2$ for large range of Ri values. It is apparent that there are more than 3 decades of variation in the values of entrainment which are reflected in a similar range of variation for the mixing efficiency. For salty interfaces the relationship between the mixing efficiency and the local Richardson number (Ri) is a function of entrainment as

$$\eta = ERi = Ri^{1-n} = Ri^{-1/2}. \tag{14}$$

For heat stratified experiments, on the other hand, the mixing efficiency does not seem to depend on Richardson number as shown in [16] in the case of steady input (for example in the grid stirred experiments). Other effects, such as the proximity of a boundary layer were shown to affect the results [26]. See in fig. 20 a compilation of experiments. The mixing across a density interface may be evaluated by a general entrainment law [16, 26, 35] as

$$E = \frac{Ue}{u'} = c(Pr) \cdot Ri^{-n(Ri,Pr)}. \tag{15}$$

A compilation of results as a function of the local Reynolds and Richardson's numbers is shown in fig. 21, the results for each experiment [16] (fig. 21 (right)) is only a small region of the possible parametric map. Note that the results would fit better if the local values of the parameters instead of their bulk values are known, the dots and open circles correspond to the experiments of Koop and Browand [29] and Van Atta *et al.* [10, 28].

The experiments shown in figs. 15-17 correspond to values of the Reynolds number 5000 and of the Richardson number between 2 and 20. Most of the experiments fit in the overall instability frame when local values are used, but these are often difficult to evaluate.

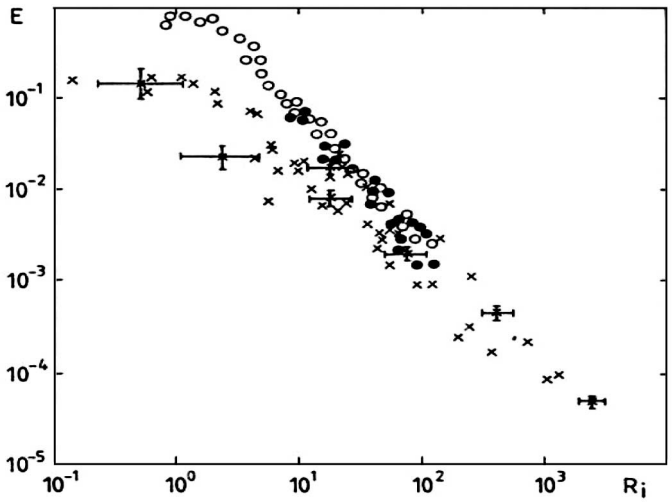

Fig. 20. – Direct measurements of entrainment as a function of the local Richardson number for these experiments the interface remains sharp. Open circles [35], closed circles [16], crosses [26] are experiments near a flat boundary.

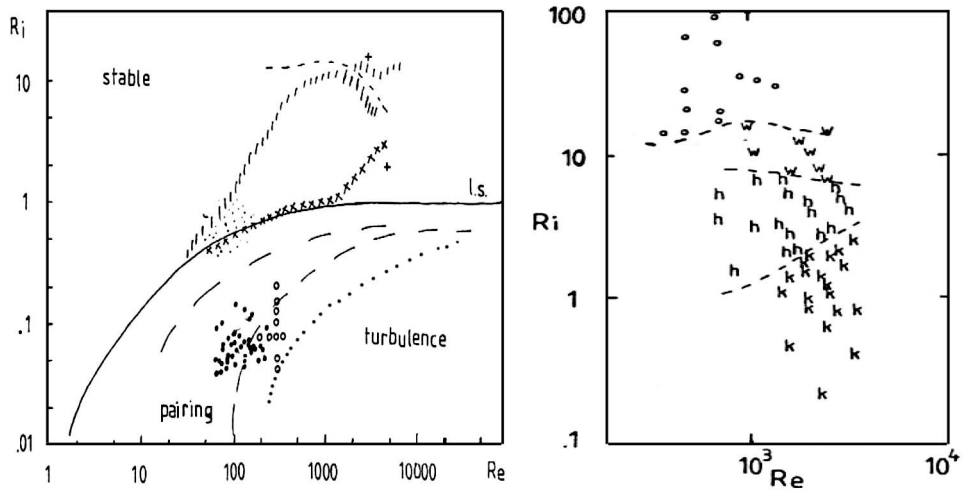

Fig. 21. – Parameter space of a stratified non-rotating flow from Redondo [10]. A general instability map with dots and circles as the experiments of [29, 30] (left). Zoom of the right upper region (right) of the parameter space (Re, Ri) where the symbols correspond to different dominant instabilities: o—no turbulence; w—internal waves; h—Holmboe waves; k—Kelvin-Helmholtz billows (right).

6. – Conclusions

The entrainment is a complex power function of the local Richardson number, and the value of the empirical exponent $n(Ri, Pr)$ is compared with previous results. The relationship between the flux Richardson number and the gradient or local one and the

ways in which the interface extracts energy from the turbulence source via internal waves is a complex non-linear function. Internal gravity (or buoyancy) waves are characteristic of the stable boundary layer and contribute to its transport processes, both directly, and indirectly via internal wave-induced turbulence. These processes are able to control entrainment across strong density interfaces as those defined by Turner [35]. A comparison of the range of entrainment values from laboratory experiments with those occurring in nature, both in the atmosphere and in the ocean, shows the importance of modelling correctly the integral length scales of the environmental turbulence.

Internal wave measurements in laboratory experiments on a linearly stratified tank match rather well the LES numerical results of the collapse of a bar wake, but also show the complexity of the non-linear internal waves. The initial growth of the wakes is quite well understood, but the subsequent collapse and in particular, how the internal waves affect mixing efficiency, is not resolved yet. Results of performed experiments with Schlieren observations of flow fields generated by oscillating and uniformly moving obstacles of different conditions are still necessary. Only in very controlled situations such as the re-circulating shear-stratified flume it is possible to identify the individual instabilities that lead to turbulent mixing. From a statistical point of view the non-homogeneity of the processes leads also to intermittency [36-38], but due to the improvement of image analysis techniques, now it is possible to evaluate multifractal and spectral indicators of the mixing processes. Even simple measurements like the thickness of the mixing layer as a function of local conditions leads to important new data as seen in eqs. (12) and (15).

Remote-sensing instruments have revealed very important features of environmental flows and their evolution. For local or global studies it is necessary to evaluate vertical mixing as these are supposed to eventually control climate change. A combination of all methods: analytical, numerical, field observations and laboratory modelling are needed.

* * *

We acknowledge the help of Profs. A. Babiano and R. Kiehn. Thanks are also due to ERCOFTAC (SIG 14) and the MINCIIT ESP2005-07551 and the E.U. ERBIC15-CT96-0111, INTAS, ISTC-148, ESA AO-IP2240 Projects for funding parts of this research.

REFERENCES

[1] Thorpe S. A., *Philos. Trans. R. Soc. London, Ser. A*, **286** (1977) 125.
[2] Ruddick B. R., McDougall T. J. and Turner J. S., *Deep-sea Res.*, **36** (1989) 597.
[3] Phillips O. M., *The Dynamics of the Upper Ocean*, 2nd edition (Cambridge University Press, Princeton) 1977.
[4] Posmentier E. S., *J. Phys. Oceanogr.*, **7** (1977) 298.
[5] Linden P. F., *Geophys. Astrophys. Fluid Dyn.*, **13** (1979) 3.
[6] Ozmidov R. V., *Atmos. Ocean. Phys.*, **8** (1965) 853.
[7] Redondo J. M. and Linden P. F., *Appl. Sci. Res.*, **59** (1998) 89.
[8] Redondo J. M. and Cantalapiedra I. R., *Appl. Sci. Res.*, **51** (1993) 217.
[9] Miles J. W. and Howard L. N., *J. Fluid Mech.*, **20** (1964) 331.
[10] Itsweire E. C., *Phys. Fluids*, **27** (1984) 764.
[11] Rai M. M. and Moin P., *J. Comput. Phys.*, **96** (1991) 15.
[12] Smagorinsky J., *Mon. Weather Rev.*, **91** (1963) 99.
[13] Lesieur M. and Metais O., *Annu. Rev. Fluid Mech.*, **28** (1996) 45.
[14] Piomelli U., Moin P. and Ferziger J. H., *Phys. Fluids*, **31** (1898) 1884.

[15] Gonzalez-Nieto P. L., Cano D., Cano J. L. and Tijera M., these proceedings.
[16] Redondo J. M., *The Structure of Density Interfaces*, Ph. D. Thesis, CUP, University of Cambridge (1990).
[17] Mitkin V. V., Prokhorov V. E. and Chashechkin Y. D., *Fluid Dyn.*, **33** (1998) 303.
[18] Mitkin V. V., *Atmos. Ocean. Phys.*, **37** (2001) 78.
[19] Rohr J. J. and Van Atta C. W., *J. Geophys. Res.*, **92** (1987) 5481.
[20] Moum J. N., *J. Geophys. Res.*, **101** (1996) 14095.
[21] Berraba S., Fraunie P. and Crochet M., *Sci. Comput. Appl.*, **7** (2001) 12.
[22] Redondo J. M. and Metais O., *Mixing in Geophysical Flows* (CIMNE, Barcelona) 1995.
[23] Yague C., Viana S., Maqueda G. and Redondo J. M., *Non-Linear Proc. Geophys.*, **13** (2006) 185.
[24] Vindel J. M., Yague C. and Redondo J. M., *Non-Linear Proc. Geophys.*, **15** (2008) 915.
[25] Vindel J. M., Yague C. and Redondo J. M., these proceedings.
[26] Redondo J. M., *J. Hazardous Mater.*, **16** (1987) 381.
[27] Redondo J. M., Sánchez M. A. and Cantalpiedra I. R., *Dyn. Atmos. Oceans*, **24** (1996) 107.
[28] Itsweire E. C., Helland K. N. and Van Atta C. W., *J. Fluid Mech.*, **162** (1986) 299.
[29] Koop C. G. and Browand F. K., *J. Fluid Mech.*, **135** (1979) 135.
[30] Chashechkin Y. D. and Mitkin V. V., *J. Visual.*, **10** (2007) 7.
[31] Fincham A. M., Maxworthy T. and Spedding G. R., *Dyn. Atmos. Oceans*, **23** (1996) 155.
[32] Derbyshire S. H. and Redondo J. M., *Anal. Fís., Ser. A.*, **86** (1990) 67.
[33] Redondo J. M., *IMA Conf. Ser.*, Vol. **16**, edited by Drishlet D. and Perkins R. (Clarendon Press/Elsevier, Oxford) 1996, p. 210.
[34] Redondo J. M., *IMA Conf. Ser.*, Vol. **13**, edited by Farge M., Hunt J. C. R. and Vassilicos J. C. (Clarendon Press/Elsevier, Oxford) 1993, p. 353.
[35] Turner S., *Buoyancy Effects in Fluids* (Cambridge University Press) 1973.
[36] Mahjoub O. B., Redondo J. M. and Babiano A., *J. Flow Turbul. Combustion*, **59** (1998) 299.
[37] Medina P., Sánchez M. A. and Redondo J. M., *Phys. Chem. Earth*, **26** (2001) 299.
[38] Carrillo J. A., Redondo J. M., Sánchez M. A. and Platonov A., *Phys. Chem. Earth*, **26** (2001) 305.